Water Supply

Water Supply Vol 24 No 4, 1117 doi: 10.2166/ws.2024.048

Numerical simulation and structure optimization for hydraulic performance of perforated drip irrigation emitters

Kexin Du[a,b,c], Shaobo Xing[a,b,c], Jinzhu Zhang[a,b,c,*], Ningning Liu[a,b,c], Jihong Zhang[a,b,c], Miao Li[a,b,c] and Zhenhua Wang[a,b,c]

[a] College of Water Conservancy & Architectural Engineering, Shihezi University, Shihezi, Xinjiang 832000, China
[b] Key Laboratory of Modern Water-Saving Irrigation of Xinjiang Production & Construction Group, Shihezi University, Shihezi, Xinjiang 832000, China
[c] Key Laboratory of Northwest Oasis Water-Saving Agriculture, Ministry of Agriculture and Rural Affairs, Shihezi, Xinjiang 832000, China
*Corresponding author. E-mail: xjshzzjz@shzu.edu.cn

JZ, 0000-0003-3217-4622

ABSTRACT

The perforated drip irrigation emitter (PDIE) is a novel drip irrigation emitter incorporating multiple energy dissipation mechanisms, chiefly hedging, deflection, and friction. To characterize the influences of structural parameters and vortices on the hydraulic performance of PDIE, the discharge exponent, discharge rate, and emitter unit constant were analyzed via hydraulic performance experiments and numerical simulation. The key findings are: (1) Discharge exponents of PDIE ranged from 0.478 to 0.515; average high-pressure hydraulic performance exceeded low pressure by 4.882%. (2) The four key structural parameters impacted hydraulic performance from large to small as follows: the width of the perforation (a), the angle of the scalariform perforation plate (α), the distance of the two perforations (b), and the length of the channel cavity (c). Among them, the discharge exponent changes significantly with a and α. (3) Vortex-retaining PDIE exhibited a lower emitter discharge exponent versus vortex-removed versions. However, vortices increase discharge rate and reduce energy consumption of PDIE. After optimization, the emitter discharge exponent of the PDIE with the reserved vortex is 0.461, which is relatively improved by 3.556%. This study can provide a theoretical reference for the structural design of new drip irrigation emitters and functional analysis of vortices.

Key words: hydraulic performance, key structural parameters, perforated drip irrigation emitter, structural optimization, vortex

HIGHLIGHTS

- The hydraulic performance of the perforated drip irrigation emitterr is optimized.
- Key structural parameters and the vortex were explored for their effects on the hydraulic performance of the perforated drip irrigation emitter.
- By retaining vortices and adjusting key structural parameters, the hydraulic performance of PDIE can be optimized.
- The emitter of PDIE with better hydraulic performance is put forward.

GRAPHICAL ABSTRACT

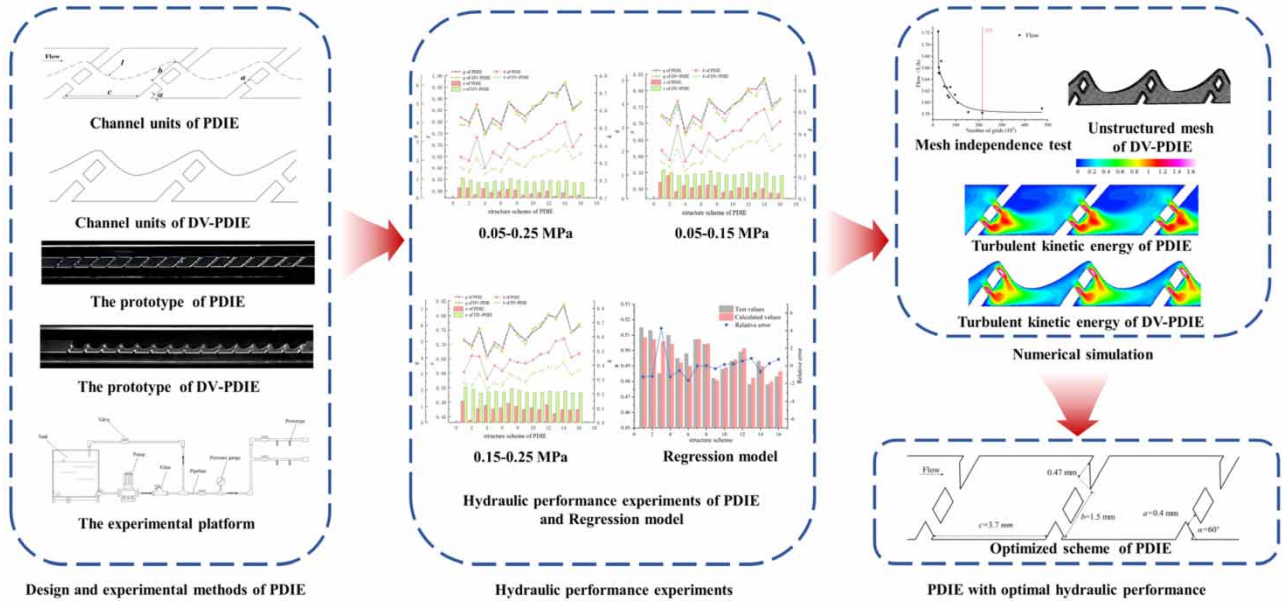

1. INTRODUCTION

Drip irrigation is one of the most efficient water-saving irrigation methods globally (Madramootoo & Morrison 2013; Lamm *et al.* 2021). Drip irrigation emitters typically dissipate flow energy by deflecting it through intricate channel boundaries, thereby enhancing the uniformity of drip irrigation systems (Sole-Torres *et al.* 2019). Compared with conventional straight-channel emitters, labyrinth channel drip emitters that rely primarily on deflection for energy dissipation have less complex manufacturing processes and relatively stable output flows. This has rendered labyrinth channel the most extensively implemented drip emitter (Li 2007).

Researchers have optimized labyrinth channel structures through physical experiments and numerical simulations to further improve hydraulic performance (Wei *et al.* 2006a, 2006b, 2007; Feng *et al.* 2020). Zhangzhong *et al.* (2016) tested various fractal channel configurations and reported significant differences in turbulence intensity. The emitter discharge exponent was greater than 0.5. Wang *et al.* (2021) proposed that adding internal teeth in the lateral channel's vortex-free zones improved hydraulic performance based on computational fluid dynamics (CFD) simulations. However, doing so in vortices diminished their area, reducing the hydraulic performance of the labyrinth channel. Yan *et al.* (2007) demonstrated that energy dissipation within labyrinth channels primarily takes place in the posterior tooth zone and channel cusps. However, even after optimization, the labyrinth emitter discharge exponent remained above 0.5.

The labyrinth channel relies primarily on flow deflection for energy dissipation. However, besides deflection, water can dissipate energy through multiple mechanisms. Incorporating these hydraulic principles could further improve performance (Yang *et al.* 2020). Moreover, large vortices do not fully utilize the labyrinth channel's internal space to dissipate energy (Zhang *et al.* 2011).

Accordingly, researchers have recently proposed new emitter designs with enhanced performance compared to labyrinth channels. Triangular circulation drip irrigation emitters (TCDIE) were designed based on fluid mechanics principles like triangular flow, sudden pipeline contractions, and expansions. The emitter discharge exponent of TCDIE was under 0.5 (Wang *et al.* 2011). Circular water-retaining labyrinth channels (CWRLC), designed around roundabouts and analyzed by CFD, also exhibited better hydraulic performance than toothed labyrinth channels (Li *et al.* 2022). Pit drip irrigation emitter employed shunting, reflux, and sharp turns for energy dissipation, inspired by plant xylem tracheid pits. Despite improved anticlogging performance compared to the labyrinth channel, their emitter discharge exponent was similar (Xu & Zhang 2020). However, manufacturing these novel emitters is more complex compared to labyrinth designs, while providing limited hydraulic performance improvements.

Therefore, Xing *et al.* (2021a) proposed an even simpler perforated drip emitter (PDIE) based on bionics and plant xylem scalariform perforation and analyzed the energy dissipation mechanism of PDIE. PDIE demonstrated enhanced hydraulic performance over the labyrinth channel (Schulte *et al.* 1989, 1999). It incorporates multiple dissipation mechanisms, chiefly hedging, sudden contraction, and sudden expansion. They proposed hydraulic performance strongly correlated with the flow ratio between the perforated channel's two main streams. However, the influence of the key structural parameters on PDIE hydraulic performance remains unclear.

Like the labyrinth channel, the perforated channel of PDIE contains mainstream and vortex, as evidenced by PDIE velocity distribution diagrams (Xing *et al.* 2021a). Some studies have examined vortex effects on the hydraulic performance of emitters. Li *et al.* (2022) proposed low-speed vortices enhance energy dissipation of channels and larger vortex areas improve emitter performance. Feng *et al.* (2018) put forward the idea of cleaning the wall of emitters by vortex. They think that emitters can have a good self-cleaning and anticlogging ability by making full use of the cleaning effect of the vortex on the wall. Wang *et al.* (2021) optimized the structure of the rectangular labyrinth channel by adding internal teeth in the vortex area. They posited that intensifying and multiplying vortices significantly increase flow energy consumption and improve hydraulic performance. Funnel-shaped drip irrigation emitters avoid particulate deposition at vortex centers through large eddy currents while still dissipating energy (Wang *et al.* 2023). However, the influence of vortices within perforated channels of PDIE hydraulic performance remains unclear.

In summary, the objectives of this study are twofold: (1) analyze the influence of key structural parameters on the hydraulic performance of PDIE, and establish a mathematical model that defines the relationship between key structural parameters and the hydraulic performance of PDIE; (2) elucidate vortex mechanisms influencing the hydraulic performance of PDIE. The ultimate goal is to determine the optimal structure for PDIE based on the impact of key structural parameters and vortex on its hydraulic performance, thereby enhancing its hydraulic performance and usability in drip irrigation systems.

2. MATERIALS AND METHODS

2.1. Structural parameters of the channel in PDIE

The perforated channel of PDIE consists of 15 units. The depth of the perforated channel is 0.80 mm, the width is 2.76 mm, and the length is 60.0 mm. The length of two perforations is 0.5 mm.

There is a large vortex and two smaller vortices in the flow field of PDIE revealed by numerical simulation. The area occupied by the large vortex was found to be significantly much larger than that of two smaller vortices, making it the primary contributor to energy consumption and steady flow in the vortices of PDIE (Xing *et al.* 2021b). Therefore, the hydraulic performance test and numerical simulation of the PDIE structure with the removal of a large vortex are carried out. The large vortex area is hereinafter referred to as the vortex. The structure diagram of the de-vortex of perforated drip irrigation emitters (DV-PDIE) is shown in Figure 1(b). The DV-PDIE model is obtained by drawing the vortex boundary by spline fitting techniques on the outermost streamline of the vortex area within the eighth unit of the perforated channel, under 0.10 MPa (Figure 1(a)).

2.2. Numerical simulation and physical experiment

2.2.1. Structural scheme of PDIE

According to the structural characteristics and geometric relationship of PDIE, the following four key parameters were extracted and their corresponding value ranges were determined. These key parameters include the width of the perforation

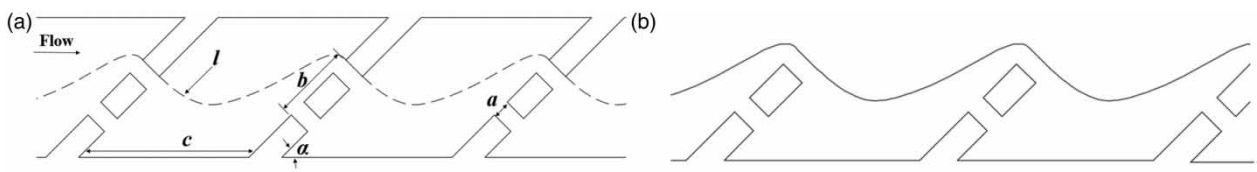

Figure 1 | Structure diagram of channel unit. (a) PDIE. (b) DV-PDIE. *Note*: '*l*' represents the vortex boundary obtained by fitting the outermost streamline of the vortex area. '*a*' represents the width of the perforation, '*b*' represents the distance to the far side of the two perforations, '*c*' represents the length of the channel cavity, and '*α*' represents the angle of the scalariform perforation plate.

(a) with values of 0.25, 0.30, 0.35, and 0.40 mm; the distance to the far side of the two perforations (b) with values of 1.20, 1.30, 1.40, and 1.50 mm; the length of the channel cavity (c) with values of 3.10, 3.30, 3.50, and 3.70 mm; and the angle of the scalariform perforation plate (α) with values of 45, 50, 55, and 60° (Ai *et al.* 2011). Based on the normalized mixed horizontal orthogonal table $L_{16}(4^5)$ in the orthogonal test design, 16 groups of PDIE channel structure parameters were designed (Hedayat *et al.* 2000). These structural schemes are detailed in Table 1.

The hydraulic performance experiment and numerical simulation are carried out for each structural scheme. The emitter discharge exponent 'x' is the most important performance index of drip irrigation emitters, which can show the hydraulic performance of drip irrigation emitters (Zhang & Gary 2012). The smaller the x is, the less sensitive the emitter discharge rate to pressure changes is (Gyasi-Agyei 2019). By conducting pressure-flow tests, the emitter discharge rate, emitter unit constant, and emitter discharge exponent for each structural scheme across different pressure ranges were obtained.

2.2.2. Numerical simulation method

To ensure accurate modeling of PDIE and DV-PDIE, SolidWorks 2018 was utilized for 3D modeling. To fully develop the flow, the length of the inlet section of the channel was appropriately extended. Fluent 2022 is used to simulate the flow of fluids in the channel of PDIE and DV-PDIE. Because the flow in the channel of drip irrigation emitters is complex and the Reynolds number is low, the uncoupled implicit algorithm, standard k-ε model, and standard wall function (Cao *et al.* 2014; Xu & Zhang 2020). The SIMPLE solver was used to couple pressure and velocity. The boundary condition of the channel inlet was set to the pressure inlet. The pressure inlet range was 0.05–0.25 MPa, and the emitter discharge rate per 0.025 MPa pressure was calculated. The boundary condition of the outlet of the channel was set to free flow (Qin *et al.* 2022).

The meshing method of PDIE was the same as the previous study (Xing *et al.* 2021a). The unstructured mesh of DV-PDIE was divided by ICEM CFD. To ensure high computational efficiency, the maximum mesh size for the fluid domain of DV-PDIE was set to 0.20, 0.19, 0.18, 0.17, 0.16, 0.15, 0.14, 0.13, 0.12, 0.11, 0.10, 0.09, 0.08, and 0.06 mm, respectively. Based on these different mesh sizes, the emitter discharge rate of DV-PDIE under the pressure of 0.10 MPa was calculated. Obtain the variation of the simulated discharge rate with the number of mesh cells. The grid independence test is shown in Figure 2(a) (Zhou *et al.* 2021). Considering the computational efficiency and accuracy, a maximum mesh size of 0.08 mm was selected to mesh the DV-PDIE finally (Xu & Zhang 2020). The total number of divided mesh is about 2.15 million, as shown in Figure 2(b).

2.2.3. The hydraulic performance experiment

The prototype utilized in the test was formed by proportionally processing the three-dimensional model using a high-precision computer numerical control (CNC) engraving and milling machine (JDVT700T, Beijing Jingdiao Group, Beijing, China) and transparent colorless plexiglass. The measurement of the prototype was conducted using an electron microscope (Motorized rotating 3D microscope, GP-490H, GAOPIN Corporation, KunShan, China) that is shown in Supplementary Materials (Figure S1). The experiment system was made up of the tank, pump, valve, filter (120 mesh filter), pressure gauge (YB-150, measuring range 0–40 MPa, 0.25 accuracy), prototype, pipeline, etc. The test platform and channel prototypes are shown in Figure 3. The pressure of the device was provided by the pump. The system employed the combined action of

Table 1 | PDIE orthogonal test schemes

	Structural parameters					Structural parameters			
Scheme	a (mm)	b (mm)	c (mm)	α (°)	Scheme	a (mm)	b (mm)	c (mm)	α (°)
1	0.25	1.2	3.1	45	9	0.35	1.2	3.5	60
2	0.25	1.3	3.3	50	10	0.35	1.3	3.7	55
3	0.25	1.4	3.5	55	11	0.35	1.4	3.1	50
4	0.25	1.5	3.7	60	12	0.35	1.5	3.3	45
5	0.30	1.2	3.3	55	13	0.40	1.2	3.7	50
6	0.30	1.3	3.1	60	14	0.40	1.3	3.5	45
7	0.30	1.4	3.7	45	15	0.40	1.4	3.3	60
8	0.30	1.5	3.5	50	16	0.40	1.5	3.1	55

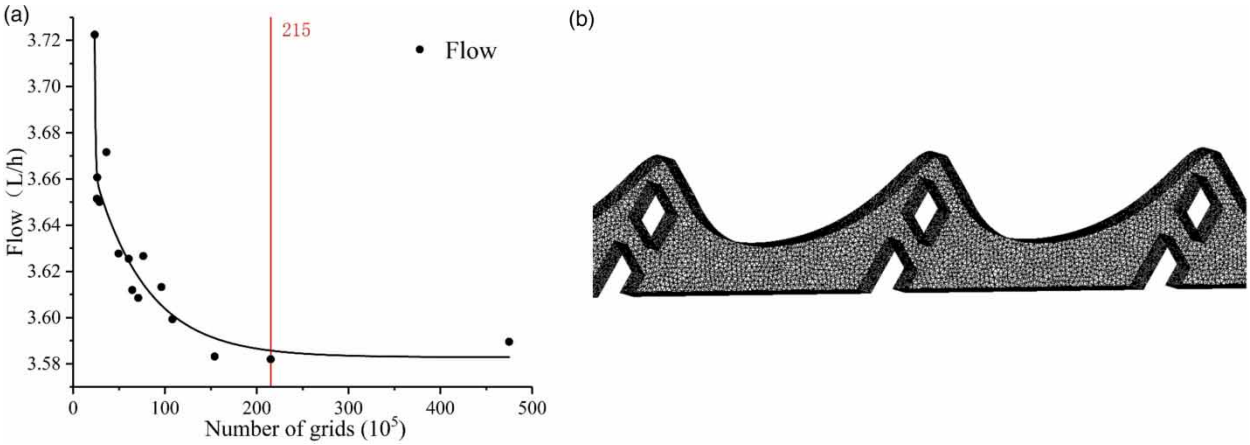

Figure 2 | Fluid domain meshing of DV-PDIE. (a) Mesh independence test and (b) unstructured mesh of DV-PDIE.

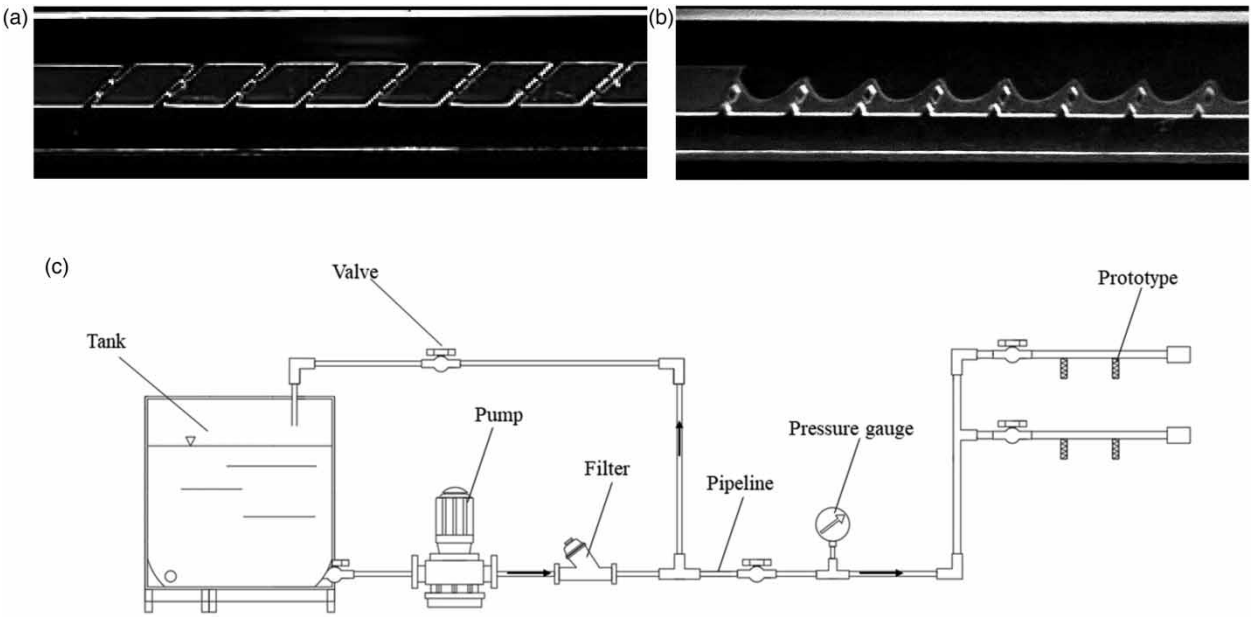

Figure 3 | Experiment platform and channel prototypes. (a) The prototype of PDIE; (b) the prototype of DV-PDIE; and (c) test platform.

two valves to regulate the inlet pressure of PDIE to measure the emitter discharge rate of PDIE at different pressures. The hydraulic performance test measured the emitter discharge rate when the inlet pressure of PDIE was from 0.05 to 0.25 MPa. In this test, the emitter discharge rate of PDIE was tested three times per 0.25 MPa pressure. Each pressure setting was tested for 5 min. The emitter discharge rate of PDIE was determined using the volumetric method, utilizing a measuring cylinder with a measurement accuracy of 0.001 L. To ensure precision, the measurements were verified using an electronic balance with an accuracy of 0.001 g.

The pressure does significantly affect the hydraulic performance of drip irrigation emitters. To investigate the hydraulic performance of both PDIE and DV-PDIE under various pressure intervals, the working pressure of emitters is divided into three ranges: low-pressure range (0.05–0.15 MPa), high-pressure range (0.15–0.25 MPa), and complete pressure range (0.05–0.25 MPa). Based on Equation (1), the emitter unit constant (k) and emitter discharge exponent (x) of each structural scheme of PDIE and DV-PDIE are calculated by Stata 16 software. The k and x are expressed as follows:

$$q = kH^x, \tag{1}$$

where q is the average emitter discharge rate in L/h, x is the emitter discharge exponent, k is the emitter unit constant, and H is the inlet pressure in MPa.

The relative error between the simulated values and test values of the emitter discharge rate for the 16 different structural schemes of PDIE ranges from 1.381 to 2.439% (Xing *et al.* 2021a). The largest and smallest differences between the simulated and test values of DV-PDIE structure emitter discharge rate are scheme 4 and scheme 10, and the relative errors are 2.316 and 1.272%, respectively. The pressure – emitter discharge rate curves of scheme 4 and scheme 10 are shown in Figure 4.

3. RESULTS

3.1. Effect of structural parameters on the hydraulic performance of PDIE

Test results of hydraulic performance are shown in Figure 5 and Supplementary Materials (Table S1–S3). The range of q, x, and k of 16 groups of PDIE are 2–8 L/h, 0.478–0.515, and 0.273–0.533, respectively. Figure 5 shows that there are differences in the emitter discharge exponent of different PDIE schemes, with a maximum difference of 0.036 and a minimum difference of 0.040. The emitter discharge exponent of the same PDIE scheme in the high-pressure range is lower than that in the low-pressure range, the maximum difference is 0.102 and the minimum difference is 0.011. This shows that the hydraulic performance of PDIE is affected by the pressure, and PDIE exhibits superior hydraulic performance in the high-pressure range.

As shown in Figure 5 and Supplementary Material (Table S1–S3), the emitter discharge rate of both DV-PDIE and PDIE increases proportionally with the increasing pressure. It is noteworthy that all schemes encompass an identical exit area. Consequently, the flow velocity of both DV-PDIE and PDIE escalates correspondingly with an upsurge in pressure. Furthermore, the observation that PDIE demonstrates enhanced hydraulic performance in the high-pressure range compared to the low-pressure range can be attributed to the concurrent increase in flow velocity within the channel as the pressure rises. This, in turn, amplifies the diverse energy dissipation phenomena present in PDIE, including the collision of two flows through the perforated plate and the merging of the mainstream area with the vortex area and so on. Consequently, PDIE exhibits superior hydraulic performance when operating at higher pressures.

The range analysis results of the structural parameters for x are shown in Table 2. The range R of the hydraulic performance experimental results for the structural parameters at different levels signifies the extent to which these structural parameters impact the hydraulic performance of PDIE. Among the investigated structural parameters, the order of the influence on x can be categorized as follows: $a > \alpha > b > c$. Within the tested value range, the PDIE structure scheme that demonstrates the optimum hydraulic performance corresponds to $a = 0.4$ mm, $b = 1.5$ mm, $c = 3.7$ mm, and $\alpha = 60°$.

Range analysis can provide an overview of the impact of structural parameters on x, and cannot solely determine to judge whether the influence of structural parameters on x is significant. To further analyze the influence of structural parameters on

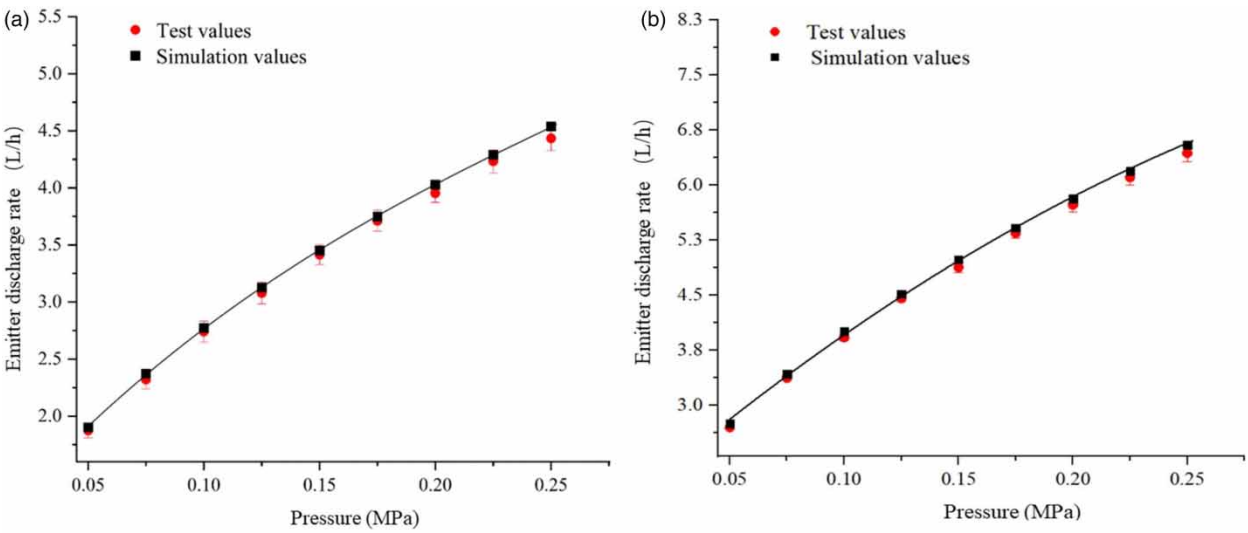

Figure 4 | Pressure–emitter discharge rate curves of structural Schemes 4 and 10. (a) DV-PDIE structure scheme 4 and (b) DV-PDIE structure Scheme 10.

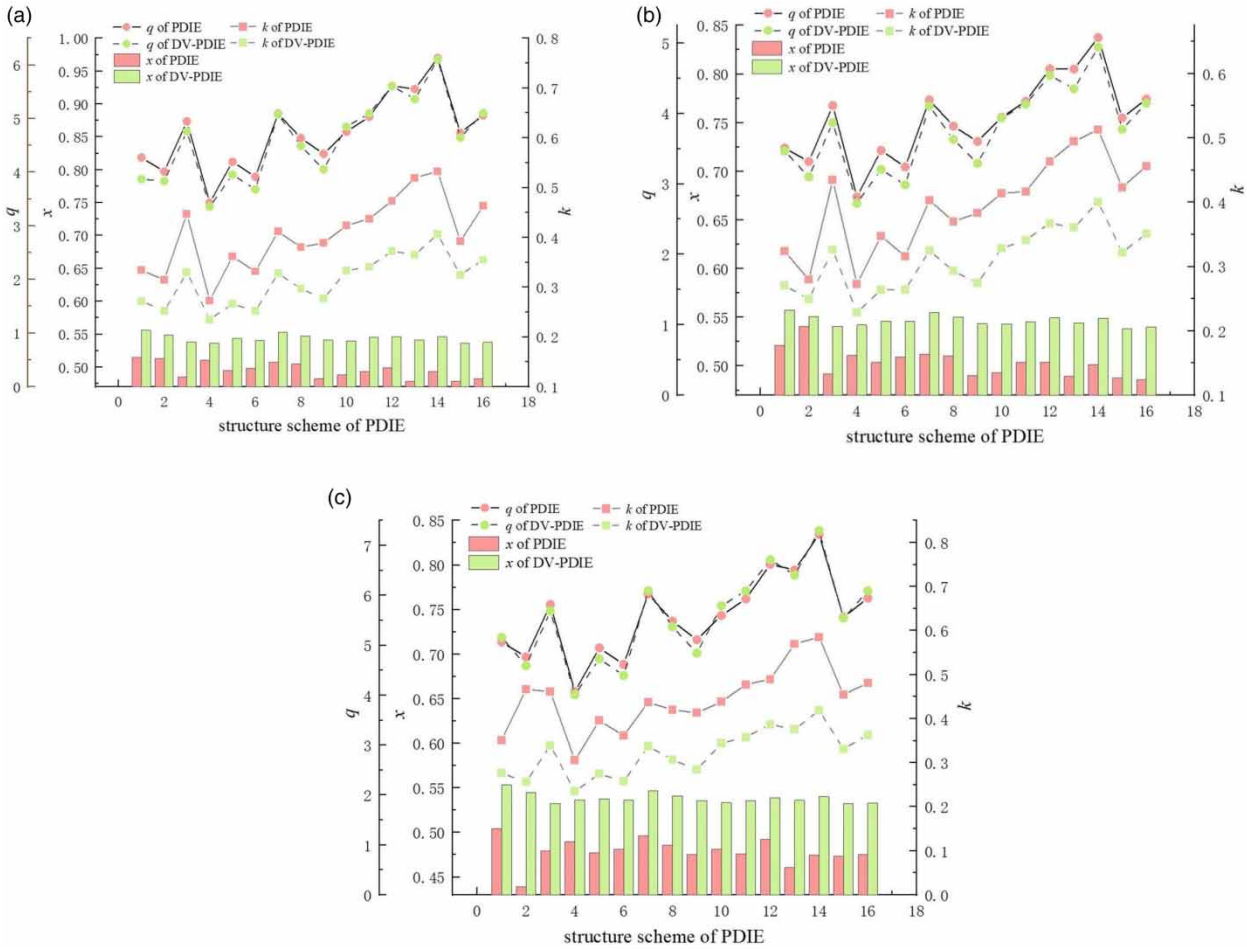

Figure 5 | Different pressure ranges *q*, *k*, and *x* of the PDIE and DV-PDIE. (a) 0.05–0.25 MPa; (b) 0.05–0.15 MPa; and (c) 0.15–0.25 MPa.

the hydraulic performance of PDIE, an analysis of variance was used to analyze the significance of the influence of key structural parameters on PDIE hydraulic performance with a significance level of 0.05. The results of the analysis of variance analysis show that parameters a and α of the PDIE have a significant effect on x, while parameters b and t c have no significant effect on x.

Table 2 | Range analysis values of emitter discharge exponents

	Structural parameters			
Range analysis values of *x*	***a* (mm)**	***b* (mm)**	***c* (mm)**	***α* (°)**
K_1	2.023	1.970	1.988	2.014
K_2	2.005	1.992	1.985	1.989
K_3	1.962	1.964	1.964	1.950
K_4	1.932	1.996	1.984	1.969
k_1	0.506	0.492	0.497	0.503
k_2	0.501	0.498	0.496	0.497
k_3	0.490	0.491	0.491	0.488
k_4	0.483	0.499	0.496	0.492
Extreme difference R	0.091*	0.032	0.024	0.063*

*The significant results of the analysis of variance of the emitter discharge exponents.

Combined with Figure 6(a), it is seen that the turbulence in the confluence area of the two streams within the perforation and behind the perforation plate is considered stronger than that in other areas of the channel. This area is the main energy dissipation area of PDIE. The parameter α changes plays a crucial role in altering various factors such as the deflection angle of the flow through the perforated plate, the hedging angle of the two streams, and the intensity of mixing between the main flow area and the vortex area. While the parameter a has the greatest influence on x among the four structural parameters. It is shown that the perforation resistance directly affected by the parameter a and the velocity of the flow through the perforation plate are the main factors that affect the steady flow of PDIE under different pressures. These findings corroborate the previous conclusion that the energy dissipation of PDIE mainly comes from the hedging and mixing of two streams (Xing *et al.* 2021a). Therefore, the influence of the width of the perforation (a) and the angle of the scalariform perforation plate (α) on the emitter discharge exponent is more significant.

To use the mathematical model to predict the hydraulic performance of PDIE under different structural parameters, based on the emitter discharge exponent of different structural schemes in the hydraulic performance test, the key structural parameters of each structural scheme were standardized by dimensional analysis method (the Buckingham Pi theorem) as shown in Equation (2).

$$f_1(x, a, b, c, \alpha) = 0. \tag{2}$$

There are five variables in Equation (2), and the basic dimension involved is length L. According to Pi theorem, the equation can be expressed into a functional relationship with four dimensionless variables as shown in Equation (3).

$$f_2(\Pi_1, \Pi_2, \Pi_3, \Pi_4) = 0. \tag{3}$$

By selecting a as the basic physical variable, Π_i can be expressed in Equation (4):

$$\begin{aligned} \Pi_1 &= x \cdot a^{\beta 1}, \\ \Pi_2 &= b \cdot a^{\beta 2}, \\ \Pi_3 &= c \cdot a^{\beta 3}, \\ \Pi_4 &= \alpha \cdot a^{\beta 4}. \end{aligned} \tag{4}$$

where β_i represents the index.

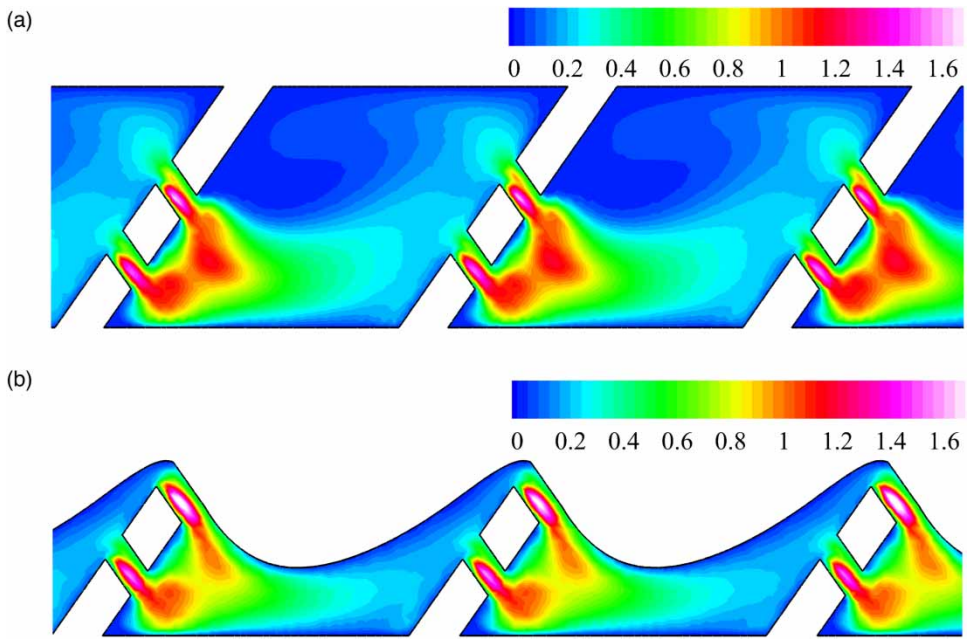

Figure 6 | Turbulent kinetic energy in 0.05–0.25 MPa for PDIE 5 and DV-PDIE 5. (a) PDIE 5 and (b) DV-PDIE 5.

Equation (4) can be expressed in a dimensional form, as shown in Equation (5).

$$\begin{aligned}[\Pi_1] &= L^0 \cdot a^{\beta 1} = L^0,\\ [\Pi_2] &= L^1 \cdot a^{\beta 2} = L^0,\\ [\Pi_3] &= L^1 \cdot a^{\beta 3} = L^0,\\ [\Pi_4] &= L^{0\cdot} \cdot a^{\beta 4} = L^0.\end{aligned} \tag{5}$$

It is obvious that β_1, β_2, β_3, and β_4 are equal to 0, -1, -1 and 0, respectively. Based on Equation (5), Equation (3) can be expressed as follows.

$$f_2\left(x, \frac{b}{a}, \frac{c}{a}, \alpha\right) = 0. \tag{6}$$

Equation (6) can be further expressed as Equation (7).

$$x = f_3\left(\frac{b}{a}, \frac{c}{a}, \alpha\right). \tag{7}$$

The corresponding regression equation was obtained by multiple regression fitting of structural parameters with x by Stata 16 base on Equation (7). The regression equation for structure parameters and x of PDIE obtained by multiple linear regression analysis is shown as Equation (8):

$$x = -0.14758\frac{b}{a} + 0.00104\frac{c}{a} - 0.000857\alpha + 0.56464. \tag{8}$$

To assess the reliability of the mathematical model, the aforementioned structural parameters are substituted into Equation (8) to calculate x for each PDIE structure scheme. To gauge the accuracy of the model, a comparison was made between the estimated values and the test values, and the resulting relative error is depicted in Figure 7 and Supplementary Materials (Table S4). The range of the x in the estimated value is 0.479–0.508, and the range of x of the test value is 0.478–0.515. The absolute range of the relative error between the estimated and the test values falls within -1.644 to 4.27%, and the average relative error is $0.871\% < 5\%$. The results of x calculated by the regression model are in good agreement with the measured values. The coincidence degree of the mathematical model is good. Therefore, it is reliable to use the mathematical model to predict the hydraulic performance of PDIE. The mathematical model can be used to predict the hydraulic performance of PDIE and optimize the structural parameters (Zhang *et al.* 2010).

3.2. The hydraulic performance of PDIE and DV-PDIE

As depicted in Figure 5 and Supplementary Materials (Table S1–S3), under the same pressure range, the average q of DV-PDIE exhibits a downward trend when compared to PDIE. Under the pressure range of 0.05–0.25 MPa, the q of DV-PDIE decreased by 2.710%, and the average decrease in q in the low-pressure range was 4.108%, which was greater than the average decrease of 0.733% in the high-pressure range. Therefore, removing the vortex area reduces q of PDIE and enhances the energy dissipation effect of the channel; especially at the low-pressure range, the effect of energy dissipation is significantly improved.

In terms of the k, it is observed that DV-PDIE exhibits a decrease in k across all pressure ranges, with an average decrease of 22.433% compared to PDIE. The average decrease of k in the DV-PDIE low-pressure range is 20.831%, while the high-pressure range is 27.352%. After removing the vortex area structure in PDIE, the x shows an opposite trend to the k.

The x values of 16 groups of DV-PDIE structure schemes are different in three pressure ranges. Their x ranges from 0.536 to 0.556. Compared with PDIE, the x of each structure scheme of DV-PDIE increases in each pressure range and increases by 8.561, 12.525, and 9.829% in low-pressure range, high-pressure range, and complete pressure range, respectively. The x of DV-PDIE in the low-pressure range and high-pressure range is 0.532–0.553 and 0.531–0.548, respectively. Similar to the PDIE structural scheme, the average hydraulic performance of DV-PDIE in the high-pressure range is 4.882% better than that in

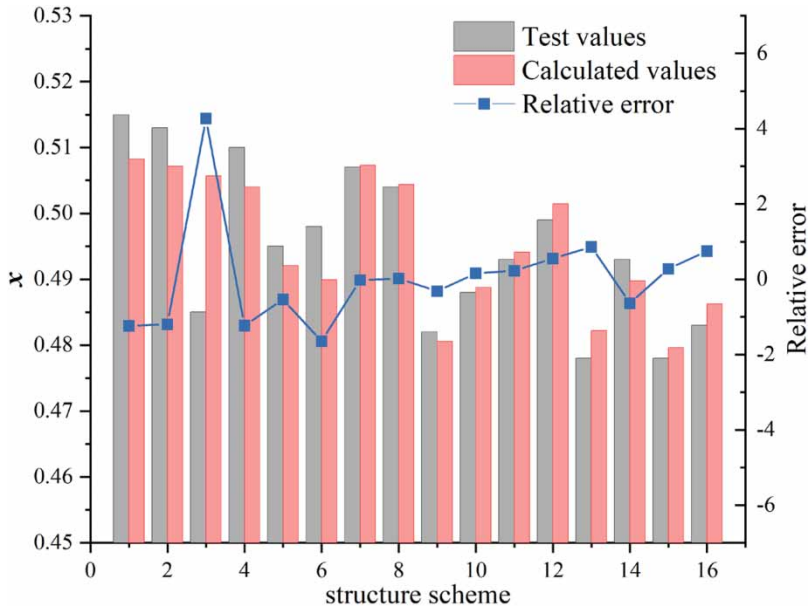

Figure 7 | Regression model calculation values and the test values of x and relative errors.

the low-pressure range. This indicates that removing the vortex area results in a decrease in the hydraulic performance of PDIE. The vortex has a steady effect on the emitter discharge exponent.

According to the velocity distribution, PDIE can be divided into a high-speed main flow area and a low-speed vortex area. Upon removal of the vortex area in PDIE, the hydraulic performance experiences a diminishing trend. The better the hydraulic performance of PDIE is, the more the percentage of emitter discharge exponent increases after the vortex area is removed. Similarly, the percentage increase of emitter discharge exponent in the high-pressure range with better hydraulic performance is also larger than that in the low-pressure range with poor hydraulic performance. This shows that the better the hydraulic performance of the working condition, the more obvious the role of the vortex area in the steady flow. This is the same as Xing's view that the vortex area stably exists under different pressures and can improve the hydraulic performance of drip irrigation emitters (Xing *et al.* 2021b).

3.3. The change of turbulent kinetic energy of PDIE and DV-PDIE

To analyze the relationship between x of PDIE and the increase of its x of corresponding DV-PDIE, the increased percentage of x of PDIE and DV-PDIE was calculated as shown in Equation (9):

$$\delta = \frac{x_2 - x_1}{x_1} \times 100\%. \tag{9}$$

where δ is the increasing percentage of the emitter discharge exponent between PDIE and DV-PDIE, x_1 is the emitter discharge exponent of PDIE at 0.05–0.25 MPa, and x_2 is the emitter discharge exponent of DV-PDIE at 0.05–0.25 MPa.

Table 3 can be generated by arranging the increase of x of DV-PDIE, after the removal of the vortex area, in a descending order and the x of PDIE in an ascending order. The analysis of Table 3 indicates a parallel distribution trend in the sequence numbers of the structural schemes for PDIE and DV-PDIE. Specifically, as the x value of PDIE decreases, the increase in the emitter discharge exponent of the DV-PDIE formed after vortex removal relative to the original PDIE becomes more obvious. This trend shows that the better the hydraulic performance of PDIE, the greater the increased percentage of the emitter discharge exponent caused by removing the vortex area.

Take Scheme 5, which exhibits a moderate reduction in x under 0.05–0.25 MPa pressure. Figures 6(a) and 6(b) depict the turbulent kinetic energy diagrams of the middle horizontal section of the eighth channel unit for PDIE 5 and DV-PDIE 5, respectively. The maximum turbulent kinetic energy of DV-PDIE 5 and PDIE 5 appears on the inside of the perforation and is 1.75 and 1.57, respectively. But for the area with higher turbulent kinetic energy at the confluence of two streams

Table 3 | The x of PDIE and δ of DV-PDIE

PDIE	x	DV-PDIE	δ (%)	PDIE	x	DV-PDIE	δ (%)
13	0.478	qw13	13.245	5	0.495	qw5	9.868
15	0.478	qw9	12.192	6	0.498	qw12	9.581
9	0.482	qw15	12.119	12	0.499	qw7	8.875
16	0.483	qw16	11.380	8	0.504	qw8	8.518
3	0.485	qw3	10.932	7	0.507	qw6	8.514
10	0.488	qw14	10.781	4	0.510	qw1	8.045
14	0.493	qw10	10.632	2	0.513	qw2	6.904
11	0.493	qw11	10.605	1	0.515	qw4	5.079

in the channel cavity, the peak value of turbulent kinetic energy and the area in this area of PDIE 5 is larger than that of DV-PDIE 5.

To further analyze the relationship between the change in average turbulent kinetic energy and x of PDIE after removing the vortex. Through Equations (10) and (11), the percentage change of the average turbulent kinetic energy of DV-PDIE and PDIE was calculated when the pressure increased from 0.10 to 0.20 MPa.

The change of the average turbulent kinetic energy of emitters is calculated as shown in Equation (10):

$$\varepsilon = \frac{m_2 - m_1}{m_1} \times 100\%. \tag{10}$$

where ε is the increase of turbulent kinetic energy, m_1 is the average turbulent kinetic energy of the emitter at 0.10 MPa, and m_2 is the average turbulent kinetic energy of the emitter at 0.20 MPa.

For each structural scheme of DV-PDIE and PDIE, the difference percentage of the increase of average turbulent kinetic energy under 0.10 and 0.20 MPa is calculated as shown in Equation (11):

$$\eta = \varepsilon_2 - \varepsilon_1. \tag{11}$$

where η is the difference of the increasing percentage of the average turbulent kinetic energy, ε_2 is the percentage of the average turbulent kinetic energy of DV-PDIE, and ε_1 is the percentage of the average turbulent kinetic energy of PDIE.

When the pressure increases from 0.10 to 0.20 MPa, the average turbulent kinetic energy of DV-PDIE 5 increases by 51.054%, while the average turbulent kinetic energy of PDIE 5 increases by 57.974%. Figure 8 shows the relation curve of δ and η of DV-PDIE and PDIE under 0.10 and 0.20 MPa, respectively. With the decrease of the percentage increase of x, the average percentage increase of turbulent kinetic energy also shows a downward trend.

The analysis of turbulent kinetic energy reveals that the turbulent kinetic energy of DV-PDIE increases faster than that of PDIE with the increase of pressure. Due to the absence of the steady flow effect of the vortex area, the flow in the DV-PDIE becomes more violently turbulent when the pressure rises. This phenomenon increases the energy dissipation in the main flow area resulting in a decrease in the emitter discharge rate and weakens the ability of the channel in the emitter to stabilize the emitter discharge rate also. This observation may explain why the hydraulic performance of DV-PDIE is inferior to that of PDIE.

3.4. Structure optimization of PDIE

This study analyzes the relationship between structural parameters and the hydraulic performance of PDIE as well as the impact of the vortex area on its hydraulic performance. The results indicate that the x of PDIE increases when the vortex area is removed. The vortex area can stabilize the q with the increase of pressure. To reduce the variation of q with water pressure, it is necessary to retain the larger vortex in PDIE.

Therefore, retaining the vortex with a larger area in PDIE is beneficial to improve the hydraulic performance and reduce the sensitivity of the emitter discharge rate to pressure. Similarly, Li *et al.* (2022) considered that the hydraulic performance of

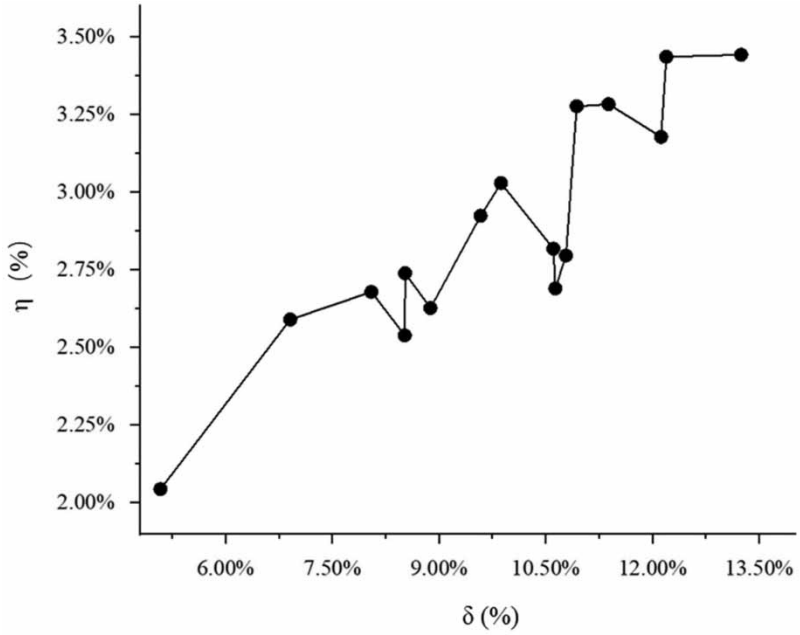

Figure 8 | The relation curve of δ and η of DV-PDIE and PDIE under 0.10 and 0.20 MPa.

CWRLC depends on the proportion of low-speed vortex area. In addition, after removing the vortex area within the PDIE, its energy consumption increases and the emitter discharge rate decreases. However, Ma *et al.* (2016) compared the hydraulic performance of the labyrinth channel with and without a vortex. They argue that the vortex can effectively reduce the emitter discharge rate of the labyrinth channel. This is contrary to the phenomenon that the emitter discharge rate decreases after the vortex is removed by PDIE. The possible reason for this difference is that the labyrinth channel mainly depends on the flow deflection to consume the energy of flow, and the existence of the vortex will enhance the deflection energy dissipation of the flow in the labyrinth channel. On the other hand, PDIE mainly relies on two mainstream hedges to consume water energy. Removing the vortex will enhance the hedging effect within the PDIE.

The best combination of hydraulic performance and structural parameters of PDIE is structure Scheme 17: $a = 0.40$ mm, $b = 1.5$ mm, $c = 3.7$ mm, and $\alpha = 60°$, combined with the energy dissipation mechanism of PDIE (Xing *et al.* 2021a) and the range of key structural parameters of this study. In addition, the upper side perforation orifice near the side wall of the channel adjusts 0.47 mm toward the wall of the channel. The optimized scheme of PDIE is shown in Supplementary Materials (Figure S2).

To further verify the relationship between the structural parameters and hydraulic performance of the aforementioned PDIE, according to the energy dissipation mechanism of PDIE 17 combined with PDIE, the test prototype of PDIE 17 was manufactured and the hydraulic performance tests were carried out. The minimum x of the original structure is 0.478, and the x of the optimized PDIE at 0. 05–0.25 MPa is 0.461, which is better than the original structure by 3.556%. The x of optimized PDIE at the low-pressure range is 0.474, and x at the high-pressure range is 0.448. The hydraulic performance of PDIE is further improved. It is proved that the relationship between the aforementioned key structural parameters and hydraulic performance is reliable.

Finally, the hydraulic performance and anticlogging performance of drip irrigation emitter affect its service life and comprehensive performance together, and there are still some problems to be studied.

(1) Combined with the hydraulic performance of PDIE, the influence of structural parameters of PDIE on anticlogging performance can be analyzed, and the response mechanism of the anticlogging performance of PDIE after vortex removal can be explored.
(2) The emitter discharge exponent merely reflects the sensitivity of the emitter discharge rate of drip irrigation emitters to changes in pressure. However, the emitter discharge rate is mainly affected by the energy dissipation of the channel.

Consequently, a PDIE structure that exhibits excellent hydraulic performance may not necessarily have a more suitable emitter discharge rate at the same time. The structure of PDIE can be further designed based on the rated discharge.

4. CONCLUSION

In this article, the influence of key structural parameters on the emitter discharge exponent of PDIE is analyzed by the test of hydraulic performance, and the effect of the vortex on the hydraulic performance of PDIE is explored by removing the structure of the vortex area.

(1) The emitter discharge exponent of 16 PDIE structure schemes ranges from 0.478 to 0.515. There are obvious differences in the emitter discharge exponent among different PDIE structure schemes. The average hydraulic performance of PDIE with the same geometric parameters in the high-pressure range is better than 4.882% in the low-pressure range.

(2) The structural parameters of PDIE affect its hydraulic performance. The influence of various structural parameters on the emitter discharge exponent is as follows: the width of the perforation (a) > the angle of the scalariform perforation plate (α) > the distance to the far side of the two perforations (b) > the length of the channel cavity (c). Among them, the change of emitter discharge exponent with a and α is significant, but the change with the increase of c and b is not significant.

(3) The vortex can reduce the sensitivity of PDIE flow to pressure and achieve the effect of stabilizing flow. However, the removal of the vortex can improve the energy dissipation in the main flow area and cause a decrease in the average emitter discharge rate. The optimized structural parameters for PDIE with the vortex area are as follows: $a = 0.40$ mm, $b = 1.5$ mm, $c = 3.7$ mm, and $a = 60°$. At the same time, the inlet of the upper side perforation in proximity to the channel's wall is adjusted by 0.47 mm toward the wall. The emitter discharge exponent of an optimized scheme of PDIE is 0.461.

ACKNOWLEDGEMENTS

This work was supported by Major Science and Technology Projects of XPCC (2021AA003), the National Natural Science Foundation of China (52279040), National Key Research and Development Projects (2022YFD1900405 and 2021YFD19008003), and the High-level Talent Project of Shihezi University (RCZK202319).

DATA AVAILABILITY STATEMENT

All relevant data are included in the paper or its Supplementary Information.

CONFLICT OF INTEREST

The authors declare there is no conflict.

REFERENCES

Ai, Q., Xu, F., Chen, Q., Chen, J. L. & Wang, P. 2011 Flow resistance characteristics of scalariform perforation plates in plant xylem vessels. *Transactions of the Chinese Society of Agricultural Machinery* **42** (8), 143–148.

Cao, W., Liu, J. & Zhu, Y. 2014 Numerical simulation of vibration pressure on the hydraulic performance of round-flow emitter. *Advanced Materials Research* **1073–1076**, 2205–2209.

Feng, J., Li, Y., Wang, W. N. & Xue, S. 2018 Effect of optimization forms of flow path on emitter hydraulic and anti-clogging performance in drip irrigation system. *Irrigation Science* **36** (1), 37–47.

Feng, J., Wang, W. & Liu, H. 2020 Study on fluid movement characteristics inside the emitter flow path of drip irrigation system using the Yellow River water. *Sustainability-Basel* **12** (4), 1319.

Gyasi-Agyei, Y. 2019 Validation of dripline emitter characteristics and pump performance curve for network analysis. *Journal of Irrigation and Drainage Engineering* **145** (4), 05019001.

Hedayat, A. S., Sloane, N. J. A. & Stufken, J. 2000 Orthogonal array: Theory and applications. *Technometrics* **42** (4), 440.

Lamm, F. R., Colaizzi, P. D. & Sorensen, R. B. 2021 A 2020 vision of subsurface drip irrigation in the U.S. *Transactions of the ASABE* **64** (4), 1319–1343.

Li, Y. K. 2007 Effects of fractal flow path designing and its parameters on emitter hydraulic performance. *Chinese Journal of Mechanical Engineering* **43** (7), 109–114.

Li, Y. F., Feng, X. Y., Liu, Y. D., Han, X. C., Liu, H. Y., Sun, Y. T., Liu, H. & Xie, Y. N. 2022 Research on hydraulic properties and energy dissipation mechanism of the novel water-retaining labyrinth channel emitters. *Agronomy-Basel* **12** (7), 1708.

Ma, J. F. & Li, Z. Q. 2016 Comparison of hydraulic performance in vortex and non-vortex channel of labyrinth emitter. *Yellow River* **38** (2), 142–144.

Madramootoo, C. A. & Morrison, J. 2013 Advances and challenges with micro-irrigation. *Irrigation and Drainage* **62** (3), 255–261.

Qin, C., Zhang, J. Z., Whang, Z. H., Lye, D. S., Liu, N. N., Xing, S. B. & Wang, F. 2022 Anti-clogging performance optimization for shunt-hedging drip irrigation emitters based on water-sand motion characteristics. *Water* **14** (23), 3901.

Schulte, P. J. 1999 Water flow through a 20-pore perforation plate in vessels of *Liquidambar styraciflua*. *Journal of Experimental Botany* **50** (336), 1179–1187.

Schulte, P. J., Gibson, A. C. & Nobel, P. S. 1989 Water flow in vessels with simple or compound perforation plates. *Annals of Botany* **2**, 171–178.

Solé-Torres, C., Puig-Bargués, J., Duran-Ros, M., Arbat, G. & Cartagena, F. R. D. 2019 Effect of different sand filter underdrain designs on emitter clogging using reclaimed effluents. *Agricultural Water Management* **223**, 105683.

Wang, X. K. & Li, J. 2011 Numerical calculation of triangle circulation drip irrigation emitters. In: *Proceedings of the 8th International Conference on Nanochannels, Microchannels and Minichannels 2010, PTS A AND B*. pp. 1003–1007.

Wang, C., Li, Z. & Ma, J. 2021 Influence of emitter structure on its hydraulic performance based on the vortex. *Agriculture-Basel* **11** (6), 508.

Wang, Y., Liu, N. N., Wang, Z. H., Tan, M. D., Xu, X. & Xing, S. B. 2023 Structure design and hydraulic performance analysis of drip emitters based on vortex energy dissipation. *Irrigation and Drainage* **73** (1), 3–15.

Wei, Q., Shi, Y., Dong, W. & Huang, S. 2006a Advanced methods to develop drip emitters with new channel types. *Applied Engineering in Agriculture* **22** (2), 243–249.

Wei, Q. S., Shi, Y., Dong, W., Gang, L. & Huang, S. 2006b Study on hydraulic performance of drip emitters by computational fluid dynamics. *Agricultural Water Management* **84** (1–2), 130–136.

Wei, Z. Y., Tang, Y., Zhao, W. & Lu, B. 2007 Rapid structural design of drip irrigation emitters based on RP technology. *Rapid Prototyping Journal* **13** (5), 268–275.

Xing, S. B., Wang, Z. H., Zhang, J. Z., Liu, N. N. & Zhou, B. 2021a Simulation and verification of hydraulic performance and energy dissipation mechanism of perforated drip irrigation emitters. *Water* **13** (2), 171.

Xing, S. B., Zhang, J. Z., Wang, Z. H. & Liu, N. N. 2021b Analysis of vortex action in perforated emitters under different working pressures. *Journal of Drainage and Irrigation Machinery Engineering* **39** (10), 1075–1080.

Xu, T. & Zhang, L. X. L. 2020 Influence and analysis of structure design and optimization on the performance of a pit drip irrigation emitter*. *Irrigation and Drainage* **69** (4), 633–645.

Yan, D. Z., Yang, P. L., Ren, S. M., Li, Y. K. & Xu, T. W. 2007 Numerical study on flow property in dentate path of drip emitters. *New Zealand Journal of Agricultural Research* **50** (5), 705–712.

Yang, B., Wang, J. D., Zhang, Y. Q., Wang, H. T., Ma, X. P. & Mo, Y. 2020 Anti-clogging performance optimization for dentiform labyrinth emitters. *Irrigation Science* **38** (3), 275–285.

Zhang, L. & Gary, P. M. 2012 Relationships between common irrigation application uniformity indicators. *Irrigation Science* **30** (2), 83–88.

Zhang, J., Zhao, W. H., Tang, Y. P. & Lu, B. H. 2010 Anti-clogging performance evaluation and parameterized design of emitters with labyrinth channels. *Computers and Electronics in Agriculture* **74** (1), 59–65.

Zhang, J., Zhao, W. H., Tang, Y. P. & Lu, B. H. 2011 Structural optimization of labyrinth-channel emitters based on hydraulic and anti-clogging performances. *Irrigation Science* **29** (5), 351–357.

Zhangzhong, L. L., Yang, P. L., Li, Y. K. & Ren, S. M. 2016 Effects of flow path geometrical parameters on flow characteristics and hydraulic performance of drip irrigation emitters. *Irrigation and Drainage* **65** (4), 426–438.

Zhou, B., Hou, P., Xiao, Y., Song, P., Xie, E. & Li, Y. K. 2021 Visualizing, quantifying, and controlling local hydrodynamic effects on biofilm accumulation in complex flow paths. *Journal of Hazardous Materials* **416**, 125937.

First received 29 September 2023; accepted in revised form 28 February 2024. Available online 13 March 2024